THE JOURNAL OF BIOLOGICAL CHEMISTRY
Vol. 277, No. 10, Issue of March 8, pp. 7684–7693, 2002

Printed in U.S.A.

The Ducky Mutation in *Cacna2d2* Results in Altered Purkinje Cell Morphology and Is Associated with the Expression of a Truncated α2δ-2 Protein with Abnormal Function*

Received for publication, September 28, 2001, and in revised form, December 3, 2001
Published, JBC Papers in Press, December 26, 2001, DOI 10.1074/jbc.M109404200

Jens Brodbeck, Anthony Davies, Jo-Maree Courtney, Alon Meir‡, Nuria Balaguero, Carles Canti, Fraser J. Moss, Karen M. Page, Wendy S. Pratt, Steven P. Hunt§, Jane Barclay¶‖, Michele Rees¶, and Annette C. Dolphin**

From the Departments of Pharmacology and §Anatomy and Developmental Biology, University College London, Gower Street, London WC1E 6BT and ¶Department of Paediatrics and Child Health, Royal Free and University College Medical School, The Rayne Institute, 5 University Street, London WC1E 6JJ, United Kingdom

The mouse mutant ducky, a model for absence epilepsy, is characterized by spike-wave seizures and cerebellar ataxia. A mutation in *Cacna2d2*, the gene encoding the α2δ-2 voltage-dependent calcium channel accessory subunit, has been found to underlie the ducky phenotype. The α2δ-2 mRNA is strongly expressed in cerebellar Purkinje cells. We show that *du*/*du* mice have abnormalities in their Purkinje cell dendritic tree. The mutation in α2δ-2 results in the introduction of a premature stop codon and predicts the expression of a truncated protein encoded by the first three exons of *Cacna2d2*, followed by 8 novel amino acids. We show that both mRNA and protein corresponding to this predicted transcript are expressed in *du*/*du* cerebellum and present in Purkinje cells. Whereas the α2δ-2 subunit increased the peak current density of the $Ca_V2.1/\beta_4$ channel combination when co-expressed *in vitro*, co-expression with the truncated mutant α2δ-2 protein reduced current density, indicating that it may contribute to the *du* phenotype.

Voltage-gated Ca^{2+} (Ca_V)[1] channels have been divided functionally into L-, N-, P/Q-, R-, and T-types (1). Each Ca_V channel is composed of a pore-forming α_1 subunit, associated at least in the case of the Ca_V1 and -2 subfamilies with an intracellular β subunit responsible for trafficking (2) and a membrane-anchored, but predominantly extracellular, α2δ subunit, whose function is less well defined (2). $Ca_V1.1$ (α_1S) is also associated with a γ subunit (γ_1), and this may be true for other Ca_V channels (3), although the neuronal γ subunits may also subserve other functions (4). The α_1 subunit determines the main biophysical properties of the channel and is modulated by the other subunits (2). Mammalian genes encoding 10 α_1, 4 β, 8 γ, and 3 α2δ subunits have been identified (1, 5, 6).

A number of spontaneous autosomal recessive mutant mouse strains have now been identified, involving mutations in each of the four different subunits that together compose a voltage-dependent calcium channel. They all have a similar phenotype that includes cerebellar ataxia and spike-wave seizures. Tottering (*Cacna1a*^{tg}) has a point mutation in $Ca_V2.1$ (α_1A) (7), and a number of alleles of this mutant have now been identified, as summarized recently (8). Lethargic (*Cacnb4*^{lh}) represents a truncation mutation of the β_4 subunit (9). Stargazer (*Cacng2*^{stg}) has a truncation mutation in the γ_2 subunit (3), although its role as a calcium channel subunit remains controversial (4, 10, 11). Finally, the two ducky alleles (*Cacna2d2*^{du} and *Cacna2d2*^{du2j}) both predict truncation mutations in the α2δ-2 subunit (12).

Homozygotes for the ducky (*du*) allele are characterized by ataxia and paroxysmal dyskinesia (13). The cerebellum is reduced in size (14), but we have previously found no loss of Purkinje cell (PC) bodies at postnatal day (P) 21 (12). In this study we observed a reduction in calcium channel current in P21 PCs isolated from *du*/*du* compared with +/+ cerebella (12). The present study provides evidence that the *du* mutation results in the persistence of PCs with an immature and grossly abnormal morphology, including multiple primary dendrites and a reduction in the size of the PC dendritic tree. This is associated with loss of full-length α2δ-2 protein and expression of a truncated mutant α2δ-2 protein with aberrant function.

EXPERIMENTAL PROCEDURES

Construction of du-mut1 α_2—The *du* mutant 1 construct (*du*-mut1 α_2) was assembled by PCR (Platinum *Pfx* polymerase; Invitrogen) of *du*/*du* total brain cDNA using primers corresponding to the cDNA sequence (GenBank™ AF247140) containing engineered *Sma*I or *Spe*I restriction sites. The primer sequences are as follows: F, 5′- TTG(CCCGGG)GAACATGGCGGTGCCCGGCT-3′, and R, 5′- TCT(CAGGTC)AGAGTAACCAGAGACCAA-3′, with the recognition sites indicated in parentheses. The PCR product was digested with *Sma*I and *Spe*I and ligated into the corresponding sites of a modified pMT2 vector (Genetics Institute, Cambridge, MA). Insert sequence fidelity was determined by automated sequencing (PE Biosystems, Warrington, UK).

Genotyping—Mice were obtained from The Jackson Laboratory (Bar Harbor, ME), and a colony was established, as described previously (12). RNA was extracted from samples of mouse brain tissue using RNeasy Mini Kit and QIAshredder (Qiagen Ltd., Crawley, West Sussex, UK). RNA was reverse-transcribed using Moloney murine leukemia virus-reverse transcriptase (Promega, Southampton, UK) with 0.6 units·ml^{-1} RNasin Ribonuclease Inhibitor (Promega) and 25 ng·μl^{-1} Random Hexamers (Promega). PCRs were carried out with primers

* This work was supported by the Medical Research Council (UK), The Wellcome Trust, and Epilepsy Research Foundation. The costs of publication of this article were defrayed in part by the payment of page charges. This article must therefore be hereby marked "*advertisement*" in accordance with 18 U.S.C. Section 1734 solely to indicate this fact.

‡ Current address: Alomone Laboratories, Jerusalem 91042, Israel.
‖ Current address: Novartis Institute for Medical Sciences, 5 Gower Place, London WC1E 6BS, UK.
** To whom correspondence should be addressed: Dept. of Pharmacology, University College London, Gower Street, London WC1E 6BT, UK. Tel.: 44-20-7679-3054; Fax: 44-20-7813-2808; E-mail: a.dolphin@ucl.ac.uk.

[1] The abbreviations used are: Ca_V, voltage-gated Ca^{2+}; Ab, antibody; FL, first latency; ML, molecular layer; PBS, phosphate-buffered saline; PC, Purkinje cell; PCL, Purkinje cell layer; CHAPS, 3-[(3-cholamidopropyl)dimethylammonio]-1-propanesulfonic acid; DAPI, 4,6-diamidino-2-phenylindole; P, postnatal day; GFP, green fluorescent protein.

49F, 5′-ACGCCCGCTCTTGCTCTTGCT-3′, and 11R, 5′-CCTCCAAAAATCCGCATCAC-3′, which produce a 156-bp product from both the wild-type and *du* alleles of the *Cacna2d2* transcript. Primers 49F and 50R, 5′-TCAGCCTTGGCATCGTAGTA-3′, produce a 387-bp product from the wild-type allele only. Primers 20F, 5′-GCCGCATCTTGAATGGAAAC-3′, and 86R, 5′-CAGAGACCAATGAGACTGGA-3′, produce a 456-bp product from the *du* allele only.

DNA was extracted by incubating 2 mm of tail-snip tissue in 75 μl of 25 mM NaOH, 0.2 mM Na_2EDTA at 95 °C for 30 min followed by cooling to 4 °C and addition of 75 μl of 40 mM Tris-HCl. 5 μl of the resultant solution was amplified in the PCRs. Primers 98F, 5′-ACCTATCAGGCAAAAGGACG-3′, and 120R, 5′-AGGGATGGTGATTGGTTGGA-3′, produce a fragment of 541 bp from a region that is duplicated in the *du* allele. Digestion with *Bsp*HI results in two fragments of 286 and 273 bp from the *du* allele, whereas the wild-type allele remains uncut. Wild-type mice can be identified by the presence of a single band upon agarose gel electrophoresis. Heterozygous and *du*/*du* mice each show two bands and can by distinguished on the basis of their relative intensities.

Lucifer Yellow/Neurobiotin Injection and Quantification—P21-P26 mice were asphyxiated with CO_2, and the cerebella were sliced parasagitally at 400 μm in artificial cerebrospinal fluid (in mM: 125 NaCl, 25 $NaHCO_3$, 25 glucose, 2.5 KCl, 1.25 NaH_2PO_4, 2 $CaCl_2$, 1 $MgCl_2$, saturated with 95% O_2/5% CO_2 at 4 °C) using a vibratome (Campden Instruments, London, UK). Dendrites and somata of PCs were visualized by infrared differential interference contrast video microscopy (15). Glass microelectrodes (outer tip diameter 0.3 μm) were filled with an aqueous solution of 10% lucifer yellow lithium salt (Sigma) and 10% neurobiotin (Vector Laboratories Inc., Burlingame, CA), and backfilled with 1 M LiCl. Dye was injected iontophoretically into PC somata, by alternating the current repeatedly from −40 to +40 nA over 5 min. The tissue slices were then fixed for 1 h in 4% paraformaldehyde, stained for neurobiotin with Texas Red-coupled streptavidin (Molecular Probes, Eugene, OR, 25 $\mu g \cdot ml^{-1}$ for 1 h), and viewed by confocal microcopy.

Four cells of two genotypes (+/+ and *du*/*du*) were scanned using identical parameters. Selected fields were optically sectioned using 1-μm steps. The entire *z* series was projected as a single composite image by superimposition. The final image was thresholded to form a binary image for analysis by NIH Image J software version 1.62. Following formation of the skeleton, the dendritic tree was contained in a minimal rectangle, and the number of dendrites were counted crossing a horizontal and diagonal line. Branch points were determined from the soma to the end of the three longest dendrites for each cell.

Golgi-Cox Staining—P24 mice were asphyxiated with CO_2, and their brains were removed from the cranium, immediately immersed in 20 ml of fixative (34 mM $K_2Cr_2O_7$, 37 mM $HgCl_2$, and 23 mM K_2CrO_4), and left undisturbed for 12 weeks in the dark at 4 °C. Vibratome sections (100 μm) were developed for 20 min in a 5% Na_2SO_3 solution, before being mounted on microscope slides and coverslipped with Vectashield (Vector Laboratories). Slides were viewed on a Leica microscope using 64× magnification. Image sections were grabbed through an attached CCD camera, using Vision Explorer software (Alliance Vision, Mirmande, France), enabling the deconvolution and projection of different optical planes.

In Situ Hybridization and Immunohistochemistry—Mice (aged P21 to P24) were anesthetized by CO_2 inhalation or pentobarbitone injection (200 $mg \cdot kg^{-1}$, intraperitoneal) and perfused intracardially with 4% paraformaldehyde in phosphate-buffered saline (PBS). The brain was placed in 4% paraformaldehyde at 4 °C for 3 h and then transferred into 30% sucrose overnight, before embedding in Cry-M-Bed (Bright Instrument Ltd., Huntingdon, UK) and sectioning. Alternatively, the brain was removed without fixation and frozen in liquid nitrogen. 10–25-μm cryostat sections were cut and air-dried onto positively charged slides (Merck).

A cDNA fragment corresponding to *Cacna2d2* 5′ (nucleotides 206–620, using the numbering system from GenBank™ accession number AF247139) was subcloned into pBluescript SK+ (Stratagene, La Jolla, CA). Sense and antisense RNA probes were prepared using T3 or T7 polymerase and digoxigenin RNA labeling mix and purified using Quickspin columns (Roche Molecular Biochemicals). *In situ* hybridization was carried out as described (16).

Two polyclonal antipeptide antibodies were raised in rabbits to amino acids 16–29 and 102–117 of α2δ-2. Neither of the peptides used as antigens showed any homology with other protein sequences in the data base. They were purified by affinity chromatography using the immobilized synthetic peptide and stored at 0.5 $mg \cdot ml^{-1}$ in PBS, pH 7.2, at −20 °C. For immunohistochemistry of α2δ-2, 25-μm sections were incubated overnight with primary antibody at 4 °C (1.25 $\mu g \cdot ml^{-1}$). This was followed by a biotinylated anti-rabbit IgG secondary antibody (Sigma, 7.2 $\mu g \cdot ml^{-1}$) and a Texas Red-streptavidin conjugate (2 $\mu g \cdot ml^{-1}$). Some tissue sections or cells were also incubated for 1 min with the nuclear dye 4′,6-diamidino-2-phenylindole (DAPI, 300 nM, Molecular Probes). They were examined by laser scanning confocal microscopy, using 1-μm optical sections. For peptide controls the appropriately diluted antibody was incubated for 1 h at 37 °C with a 10× higher concentration (w/v) of the immunizing peptide, before applying it to sections.

Transfection of COS-7 Cells—Transfection was performed with GenePORTER transfection reagent (Gene Therapy Systems, San Diego, CA). Cells were plated onto coverslips or dishes, 2–3 h prior to transfection. The DNA and GenePORTER reagent (6 μg and 30 μl, respectively) were each diluted in 500 μl of serum-free medium, mixed, and applied to the cells. After 3.5 h, 1 ml of medium containing 20% serum was added to the cells, which were then incubated at 37 °C for 3–4 days. For electrophysiological recordings, cells were re-plated 1–6 h prior to use.

Immunocytochemistry on COS-7 Cells—The method used is essentially as described previously (17). Cells were fixed with 4% paraformaldehyde in PBS for 15 min at room temperature. For permeabilization, cells were incubated twice for 7 min in a 0.02% solution of Triton X-100 in Tris-buffered saline; otherwise, cells were washed twice with Tris-buffered saline for the same period. The primary antibodies were used at 1.25 $\mu g \cdot ml^{-1}$. The biotinylated anti-rabbit IgG secondary antibody (7.2 $\mu g \cdot ml^{-1}$) was then incubated for 2 h at 4 °C, followed by streptavidin-Texas Red (2 $\mu g \cdot ml^{-1}$). Cells were then incubated for 1 min with DAPI (300 nM).

Preparation of Whole COS-7 Cell Lysates—COS-7 cells were transfected with either α2δ-2 or *du*-mut1 α_2 as described above. On day 4 post-transfection, the cells were resuspended in detergent-free Buffer A. Samples (2 mg of total protein) were then solubilized in Buffer A containing 1% CHAPS for immunoaffinity purification of α2δ-2 as described below.

Preparation of Cerebellar Tissue Homogenate—Cerebella, stored at −80 °C, were thawed in ice-cold Buffer A (10 mM HEPES, pH 7.4, 150 mM NaCl, 2 mM EDTA, and protease inhibitors (Complete EDTA-free, Roche Molecular Biochemicals, 1 tablet/50 ml buffer)), plus 150 mM sucrose. The tissue was homogenized, and the homogenate was centrifuged at 5000 × *g* for 10 min at 4 °C. The resultant supernatant was diluted 4 times with Buffer A, prior to detergent treatment. The protein concentration of samples was determined using either the bicinchoninic acid (BCA) assay (Perbio, Tattenhall, UK) in the presence of 0.5% SDS, or where the samples were in SDS-PAGE buffer, by a modified filter paper dye-binding assay (18).

Immunoaffinity Purification of α2δ-2 and du-mut1 α_2—Affinity-purified Ab(16–29) or Ab(102–117) (2 mg) was covalently coupled to a 1-ml column of Sepharose-NHS (Amersham Biosciences) according to manufacturer's instructions. The efficiency of coupling was assessed by SDS-PAGE. The columns were pre-washed with 200 mM glycine HCl, pH 2.4, and neutralized before first use to ensure complete removal of any residual unbound IgG. Control columns contained 2 mg of protein A-Sepharose-isolated IgG from the corresponding pre-immune rabbit sera. COS-7 cells transfected with either α2δ-2 or *du*-mut1 α_2 (2 mg of total protein) or cerebellar homogenate (+/+ or *du*/*du*, 6–20 mg of total protein) were solubilized in Buffer A (see above) containing 1% (w/v) CHAPS and placed on ice for 30 min following sonication 3 times for 10 s. The detergent extracts were cleared by centrifugation (48,000 × *g*, 20 min, 4 °C) and then applied to the relevant antibody or control IgG columns that had been pre-equilibrated with Buffer A containing 0.5% CHAPS. The lysates were recirculated through the columns using two opposing syringes for 60 min at 4 °C. Unbound material was washed from the columns in Buffer A containing 0.5% CHAPS and then Buffer A + 0.1% CHAPS. Bound proteins were eluted with 200 mM glycine HCl, pH 2.4, and then concentrated for SDS-PAGE and Western blot analysis by precipitation with 10% trichloroacetic acid followed by centrifugation (30,000 × *g*, 30 min, 4 °C). Samples of the precipitated proteins were separated on either 10 or 4–20% gradient gels under reducing conditions and then electrophoretically transferred to polyvinylidene difluoride membranes for immunodetection. The polyvinylidene difluoride membranes were blocked with 3% BSA for 3 h at 55 °C and incubated overnight with a 1:1000 dilution of either Ab(16–29) or Ab(102–117) followed by a 1:1000 dilution of goat anti-rabbit IgG-horseradish peroxidase conjugate (Bio-Rad) for 1 h at 20 °C and detected using ECL (Amersham Biosciences). The antibody and control IgG columns were neutralized and washed with 50 mM Tris, pH 7.4, 1 M NaCl, and 0.02% sodium azide and stored in PBS, pH 7.2, with 0.02% sodium azide at 4 °C.

Heterologous Expression of cDNAs and Electrophysiology—GenBank™ accession numbers of cDNAs are given in parentheses. Calcium channel expression in COS-7 cells was investigated by whole cell patch clamp recording, essentially as described previously (19), by transfection of rat Ca_V 2.1 (M64373) E1686R (20), in conjunction with rat β_4 (LO2315) and mouse α2δ-2 (AF247139, common brain splice variant, lacking exon 23 and 6 bp of exon 38 (21)) or *du*-mut1 α_2 (AF247140) cDNAs cloned into the pMT2 vector. The cDNA for green fluorescent protein (mut3 GFP) (22) was included in the transfection to identify transfected cells from which recordings were made. Transfection was performed as described above, using the ratios for α_1, β, α2δ, and GFP of 3:1:1:0.1. In the single channel experiments cDNA for β-adrenergic receptor kinase 1 (β-ARK1), Gβγ binding domain was included in the transfections, at the same concentration as the β subunit cDNA (23). For expression in *Xenopus* oocytes, cDNAs encoding rabbit Ca_V 2.1 (X57689), rat β_4 and mouse α2δ-2 or *du*-mut1 α_2 cDNAs were injected intranuclearly as described previously (24), except that 4 nl of the 1:1:1 ratio cDNA mixture was injected at 1 $\mu g \cdot \mu l^{-1}$. In control experiments where α2δ-2 was omitted, the ratio was made up with buffer. Recordings were made using two-electrode voltage clamp as described previously (24), using 10 mM Ba^{2+} as charge carrier. Individual I–V relationships were fitted with a modified Boltzmann Equation 1,

$$I = G_{max}(V - V_{rev})/(1 + \exp(-(V - V_{50})/k)) \quad \text{(Eq. 1)}$$

where G_{max} is the maximum conductance; V_{rev} is the reversal potential; k is the slope factor; and V_{50} is the voltage for 50% current activation.

Single Channel Recording and Analysis—All recordings were taken from cell-attached patches on GFP-positive cells at room temperature (20–22 °C). Recording pipettes were pulled from borosilicate tubes (World Precision Instruments, Inc., Sarasota, FL), coated with Sylgard (Sylgard 184, Corning Glass), and fire-polished to form high resistance pipettes (~10 megohms with 100 mM $BaCl_2$). The bath solution, designed to zero the resting membrane potential (25), was composed of (in mM) 135 potassium aspartate, 1 $MgCl_2$, 5 EGTA, and 10 HEPES (titrated with KOH, pH 7.3), and patch pipettes were filled with a solution of the following composition (in mM): 100 $BaCl_2$, 10 tetraethylammonium-Cl, 10 HEPES, 200 nM tetrodotoxin, titrated with tetraethylammonium-OH to pH 7.4. Both solutions were adjusted to an osmolarity of 320 mosmol with sucrose. Data were sampled (Axopatch 200B and Digidata 1200 interface, Axon Instruments, Foster City, CA) at 20 kHz and filtered on-line at 1–2 kHz. Voltages were not corrected for liquid junction potential (26), measured to be −15 mV in these solutions, in order to be able to compare the results to other published material. Leak subtraction was performed by averaging segments of traces with no activity from the same voltage protocol in the same experiment and subtracting this average from each episode using pClamp6 (Axon Instruments). Statistical analysis was performed using paired or unpaired Student's t test. For the single channel analysis, patches were only used in which three or fewer overlapping openings were detected. With an open probability of about 0.5 at +40 mV and at least 20 consecutive stimulations, the number of detectable multiple openings was considered to represent the number of channels active in these patches. Event detection was carried out using the half-amplitude threshold method. Single channel amplitude was determined by a Gaussian fit to the binned amplitude distributions. Mean open and closed times were determined as a single or double exponential fitted to open time distributions. Open time distributions were only collected in episodes or parts of episodes with no overlapping openings. For closed time distributions, we used either single channel patches or segments toward the end of episodes in which only one channel remains active and no further overlaps occur. Data are expressed as mean ± S.E. For steady-state inactivation, all the available patches were considered, and each was normalized to its peak current response during the prepulse to +40 mV. Latency to first opening was measured in 2-ms bins. First latency (FL) histograms from each experiment were divided by the number of episodes collected, and the plots were then accumulated and divided by the number of stimulations, to express the data as the FL probability (23, 27). Two- and three-channel patches were also corrected for the apparent number of channels in the patch, according to Equation 2,

$$FL_1 = 1 - (1 - FL_N)^{(1/N)} \quad \text{(Eq. 2)}$$

FL_1 and FL_N are the single channel and multichannel cumulative first latency functions, respectively, and N is the apparent number of channels.

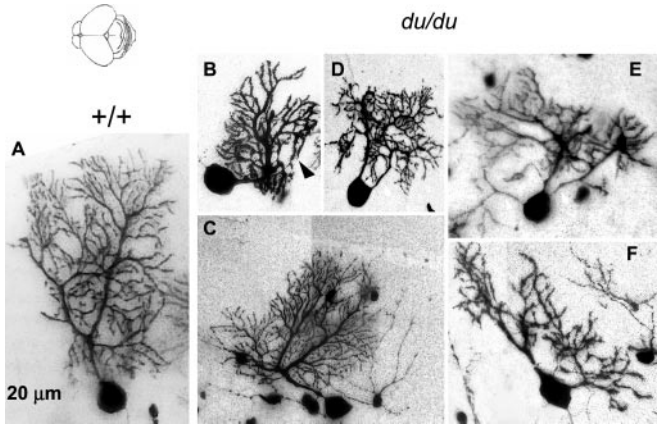

FIG. 1. **Comparison of +/+ and *du/du* PC morphology by Golgi impregnation.** Light micrographs showing individual Golgi-impregnated PCs of +/+ (*A*) and *du/du* (*B–F*) cerebellum. Parasagittal sections for both genotypes were taken from an identical region of the vermis (see *diagram top left*). *A*, typical +/+ PC with dendritic processes reaching the pial surface. *B–F*, *du/du* PCs were characterized by the absence of an apically oriented main dendrite. The cell in *B* also exhibits a weeping willow-like dendrite bending back toward the granule cell layer (*arrowhead*). The cells in *D–F* show multiple primary dendrites emerging from the perikaryon.

RESULTS

Comparison of Morphology of du/du and +/+ PCs—The *du/du* cerebellum exhibits normal foliation and laminar structure. There are no gaps in the PC layer, and their perikarya form a single row. The thickness of each layer is reduced in *du/du* compared with wild-type littermates as described previously (12). Two techniques were used to compare the morphology of cerebellar PCs between the different genotypes in more detail as follows: first, classical Golgi impregnation, and second, microinjection of PC somata with Lucifer Yellow and neurobiotin. Both methods revealed a changed PC cytoarchitecture in homozygous *du/du* cerebella at P21–26, which was the latest period in which morphology could be studied, given that the *du/du* mice die by P35. In the Golgi-impregnated cerebella, PCs were examined in detail in multiple cerebellar sections from one +/+ and six *du/du* mice. Atypical initial lateral extensions of the primary dendrite were seen in *du/du* but not in +/+ PCs (compare +/+ in Fig. 1*A* to *du/du* in Fig. 1, *B*, *C*, and *F*). The primary dendrites may then bend apically in a delayed targeting of the pial surface, which they frequently fail to reach (*e.g.* Fig. 1, *B* and *C*). Thickened tertiary branchlets were found to bend downwards in some *du/du* PCs, giving a "weeping willow" appearance (Fig. 1*B*, *closed arrowhead*). Additionally, PC somata are frequently multipolar, exhibiting up to three primary dendrites (Fig. 1, *D–F*), which, in the cells shown in Fig. 1, *E* and *F*, extend laterally rather than targeting the pial surface.

Similar results were obtained with the cell-filling technique, for which 4 +/+ and 4 *du/du* PCs were examined in detail. The *du/du* PCs displayed a dendritic arbor that was significantly less complex, reduced in size, and frequently did not reach the border of the molecular layer (compare the typical +/+ PC in Fig. 2*A* with three *du/du* PCs shown in Fig. 2*B*). Additionally, the shafts of the main and secondary dendritic branches of *du/du* PCs were often thickened (Fig. 2*B*). In one *du/du* PC, the dendrites drooped down toward the granule cell layer giving a weeping willow appearance (Fig. 2*B*, *top right panel*), similar to that seen in some of the Golgi-impregnated *du/du* PCs (Fig. 1*B*). Following formation of the skeleton of the dendritic trees (Fig. 2*C*), the numbers of dendrites were found to be reduced in *du/du* PCs (Fig. 2*D*, *left panel*), and the total length of the dendritic tree was also reduced (Fig. 2*D*, *center panel*). How-

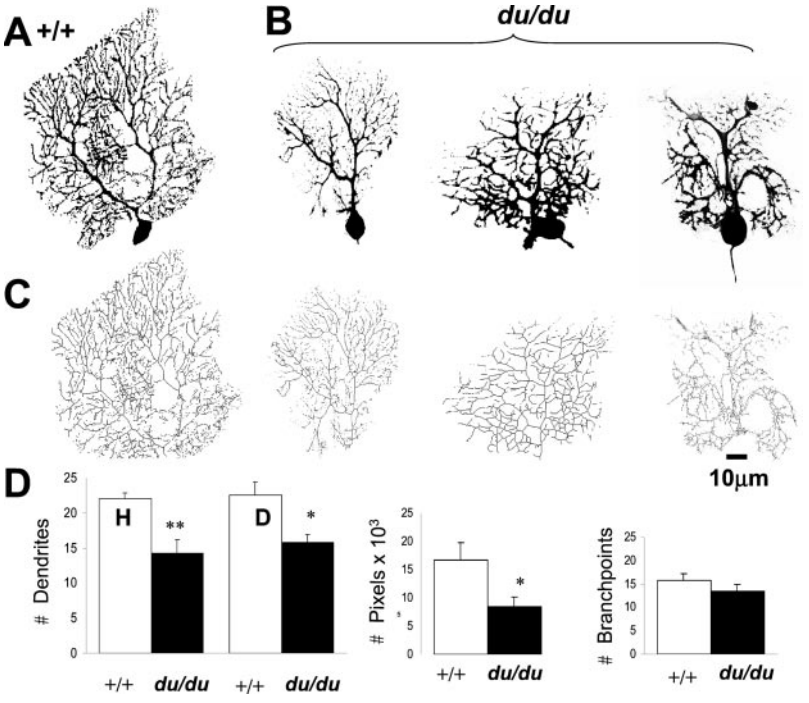

FIG. 2. **Comparison of +/+ and *du/du* PC morphology by cell filling.** Lucifer Yellow/neurobiotin injection of cerebellar PCs of +/+ (neurobiotin staining for one representative cell shown, as morphology of all +/+ PCs was similar) (*A*) and *du/du* (three cells shown, to illustrate variation in morphologies observed, the first imaged with neurobiotin staining, and the other two with lucifer yellow) (*B*). *C*, skeletonized dendritic tree of the cells, shown in *A* and *B*, for evaluation of arborization complexity, independent of dendritic width. This is quantified in *D*. *Left panel*, the number of dendrites per cell crossing a *horizontal* (*H*) and *diagonal* (*D*) *line*. *Center panel*, number of black pixels as indication of the whole area covered by skeletonized dendrites. *Right panel*, number of branch points. For all panels of *D*, $n = 4$ for both +/+ and *du/du* PCs. *Asterisks* indicate a statistically significant difference as follows: *, $p < 0.05$; **, $p < 0.01$, Student's *t* test.

ever, the number of branch points on the longest dendrites was unchanged (Fig. 2*D*, *right panel*).

The du 5′ Mutant Transcript Is Present and Translated in du/du Cerebellar PCs—We have shown previously, by *in situ* hybridization using a 3′ antisense probe, that no full-length transcript for *Cacna2d2* is present in *du/du* cerebellum, whereas a strong signal was obtained in +/+ cerebellar PCs (12). In the present study we performed *in situ* hybridization with a 5′ *Cacna2d2* antisense RNA probe to examine whether a truncated message was present in *du/du* PCs. This confirmed the presence of full-length transcript for *Cacna2d2* in +/+ PCs (Fig. 3*A*). The data would also not be inconsistent with the additional presence of transcript in small Bergmann glial cell bodies (Fig. 3*A*, *arrows*, see also Fig. 8). The results also demonstrate a low level of message hybridizing to the 5′ probe in *du/du* PCs (Fig. 3*B*, compared with Fig. 3*A*). This, together with the absence of full-length transcript in *du/du* PCs shown in our previous study (12), provides evidence for a low level of transcription of *du* mutant transcript 1 (12) in these cells.

We therefore generated an α2δ-2 antipeptide antibody utilizing an immunizing peptide corresponding to amino acids 102–117, with the intent of examining whether a mutant protein was expressed in *du/du* cerebellum. This sequence is near the N terminus of α2δ-2 and is also present in the predicted protein product of the *du* mutant transcript 1, termed *du*-mut1 α_2 (Fig. 4*A*). This antibody, called Ab(102–117), was first characterized against heterologously expressed α2δ-2. On Western blots of gels run under reducing conditions, α_2 is separated from the δ moiety to which it is disulfide-bonded under native conditions. Ab(102–117) specifically recognized the α_2 moiety of α2δ-2 (as a broad band at about 150 kDa) and not the α_2 moiety of α2δ-1 when both α2δ-1 and α2δ-2 were overexpressed in COS-7 cells (Fig. 4*B*). It also recognized an ~10-kDa protein product of the *du*-mut1 α_2 cDNA expressed in COS-7 cells (Fig. 4*B*). When Ab(102–117) was used to examine the immunocytochemical localization of α2δ-2 in these cells, the epitope was accessible in non-permeabilized cells, orienting it exofacially (Fig. 4*C*, *1st* and *2nd columns*, *upper panel*). Additional intracellular staining was observed when the cells were permeabilized (Fig. 4*C*, *1st* and *2nd columns*, *lower panel*). When *du*-mut1 α_2 was expressed, very little immunostaining was

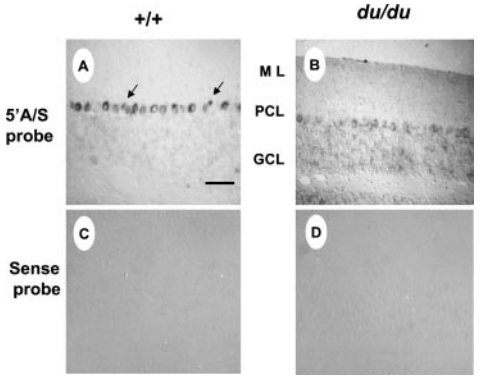

FIG. 3. **Analysis of *Cacna2d2* mutant transcript 1 expression in P21 +/+ and *du/du* cerebellum.** *In situ* hybridization of +/+ and *du/du* sections with 5′ *Cacna2d2* antisense (*A*/*S*) RNA probes designed to detect *du* mutant transcript 1 in *du/du* mice. This probe will also detect wild-type transcripts. Analyses were carried out on +/+ (*A*) and *du/du* sections (*B*). The *arrows* in *A* indicate the presence of a signal from smaller cell bodies, possibly Bergmann glial cells. No signal was detected on hybridization of control sense RNA to +/+ sections (*C* and *D*). *ML*, molecular layer; *PCL*, Purkinje cell layer; *GCL*, granule cell layer. *Scale bar*, 100 μm.

observed in non-permeabilized cells (Fig. 4*C*, *3rd column*, *upper panel*), although a large number of cells were present in the field (Fig. 4*C*, *4th column*, *upper panel*), whereas intense intracellular immunostaining, localized to intracellular organelles, was observed when the cells were permeabilized (Fig. 4*C*, *3rd* and *4th columns*, *lower panel*). The lack of staining with the anti-GFP antibody in non-permeabilized GFP-positive cells provides further evidence that the plasma membrane of the cells has not been permeabilized by fixation (Fig. 4*D*).

The predicted protein molecular mass of the entire *du*-mut1 α_2-truncated protein is 16 kDa, which is larger than the ~10-kDa band observed here. We therefore utilized another antipeptide antibody, generated against the epitope represented by amino acids 16–29, which is within the predicted signal sequence of α2δ-2, to further examine the processing of the *du*-mut1 α_2 protein. When *du*-mut1 α_2 was expressed in COS-7 cells, Ab(16–29) recognized a 16-kDa band in lysates of these cells (Fig. 5*A*, *lane 1*). No smaller molecular weight bands were

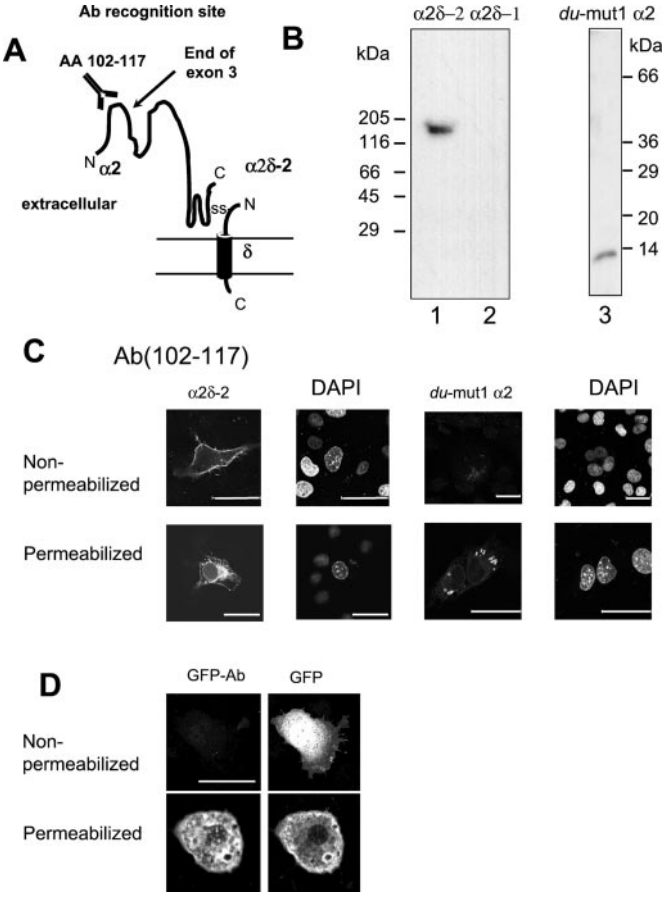

FIG. 4. **Specificity of Ab(102–117) and localization of α2δ-2 and *du*-mut1 α_2 in COS-7 cells.** *A*, schematic representation of α2δ-2 protein to show location of the Ab(102–117) binding site in relation to the end of exon 3. *B*, immunoblots to show the specificity of the anti-α 2δ-2 Ab(102–117), using lysates (20 μg of protein) from COS-7 cells overexpressing α 2δ-2 (*lane 1*, 150 kDa) or α2δ-1 as a control (*lane 2*) on 4–12% gradient SDS-PAGE gels, and *du*-mut1 α_2 (*lane 3*, ~10 kDa) on a 4–20% gel. The positions of the molecular mass markers are shown next to the blots. *C*, COS-7 cells transfected with cDNAs for GFP and α2δ-2 (*1st* and *2nd columns*) or *du*-mut1 α_2, (*3rd* and *4th columns*). Cells were either not permeabilized (*upper row*) or permeabilized with Triton X-100 (*lower row*). Immunostaining with Ab(102–117) is shown in the *1st* and *3rd columns*, and DAPI fluorescence to identify cell nuclei is shown in *2nd* and *4th columns*. For clarity, the GFP fluorescence is not shown. *D*, COS-7 cells transfected with cDNA for GFP alone. Cells were either not permeabilized (*upper row*) or permeabilized with Triton X-100 (*lower row*). GFP transfection was used as a control to show lack of immunostaining with anti-GFP Ab (*left column*) of this intracellular antigen in non-permeabilized cells. GFP fluorescence is shown in the *right column*. *Scale bar* (40 μm) applies to all sections.

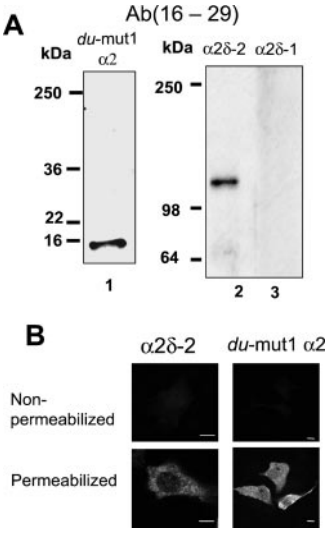

FIG. 5. **Specificity of Ab(16–29).** *A*, immunoblots to show the specificity of Ab(16–29), using lysates (20 μg of protein) from COS-7 cells overexpressing *du*-mut1 α_2 (*lane 1*, 16 kDa) on a 15% SDS-PAGE gel, or α2δ-2 (*lane 2*, 120 kDa), or α2δ-1 as a control (*lane 3*) on 4–12% gradient gels. The positions of the molecular mass markers are shown next to the blots. *B*, immunostaining using Ab(16–29) in COS-7 cells transfected cDNA for full-length α2δ-2 (*left panel*) or *du*-mut1 α_2 (*right panel*). Cells were either not permeabilized (*upper row*) or permeabilized with Triton X-100 (*lower row*), as described under "Experimental Procedures." *Scale bars*, 10 μm.

observed on this gel (but see Fig. 7). This suggested that the signal sequence of *du*-mut1 α_2 is at least partly uncleaved when it is expressed in COS-7 cells. Ab(16–29) also recognized a well defined 120-kDa protein when full-length α2δ-2 was expressed (Fig. 5*A*, *lane 2*) and no bands when α2δ-1 was expressed as a control (Fig. 5*A*, *lane 3*). This 120-kDa protein is likely to represent an immature form of α2δ-2 before cleavage of the signal sequence, which normally precedes glycosylation. The protein molecular mass of the α_2 moiety including the 6-kDa signal sequence is calculated to be 113 kDa. Unlike Ab(102–117), Ab(16–29) did not recognize a band of 150 kDa, indicating that, as expected, the signal sequence is cleaved from the mature glycosylated form of α2δ-2.

We then examined the immunolocalization of *du*-mut1 α_2 in COS-7 cells, using Ab(16–29). Immunostaining for this epitope was not observed at the plasma membrane in non-permeabilized cells expressing α2δ-2, indicating that the signal sequence is cleaved before insertion of α2δ-2 into the plasma membrane. Furthermore, this epitope was also generally not observed on the exofacial side of the plasma membrane when *du*-mut1 α_2 was expressed (Fig. 5*B*, non-permeabilized cells). Diffuse intracellular staining was observed when the cells were permeabilized, for both α2δ-2- and *du*-mut1 α_2-expressing cells (Fig. 5*B*).

Immunopurification of du-mut1 α_2 from du/du Cerebellum—The use of an Ab(102–117) immunoaffinity column allowed the isolation of a low abundance protein of ~10 kDa from *du/du* cerebellum (Fig. 6*A*, *lane 1*), which was detected using the same antibody. This protein is very similar in molecular weight to the *du*-mut1 α_2 protein isolated in the same way from lysates of COS-7 cells expressing *du*-mut1 α_2 (Fig. 6*A*, *lane 2*). If a protein product were produced from *du* mutant transcript 2 (GenBank™ accession number AF247141) in *du/du* cerebellum (12), its predicted molecular mass would be ~100 kDa. This would also be recognized by Ab(102–117), but no higher molecular weight immunoreactive bands were observed from 4 to 20% gradient gels of proteins isolated from *du/du* cerebellum (data not shown, $n = 2$). A broad band of protein of ~150 kDa, representing the α_2 moiety of α2δ-2, was isolated from +/+ cerebellum using the same immunoaffinity column and detected using the same antibody (Fig. 6*B*, *lane 1*). This protein was the same molecular weight as that isolated by the same antibody from COS-7 cells transfected with α2δ-2, with the broad band probably representing different glycosylation states (Fig. 6*B*, *lane 2*).

By using an Ab(16–29) immunoaffinity column, a protein of ~16 kDa was isolated from *du/du* cerebellum (Fig. 6*C*, *lane 1*). This protein is very similar in molecular weight to the *du*-mut1 α_2 protein isolated in the same way from COS-7 cells expressing *du*-mut1 α_2 (Fig. 6*C*, *lane 2*). Furthermore, a protein of about 120 kDa was isolated from +/+ cerebellum using the same immunoaffinity column (Fig. 6*D*, *lane 1*). This protein was the same molecular weight as that isolated by the same antibody from COS-7 cells transfected with α2δ-2 (Fig. 6*D*, *lane 2*).

The basis for the difference in molecular weight between the *du*-mut1 α_2 species recognized by the two antibodies was fur-

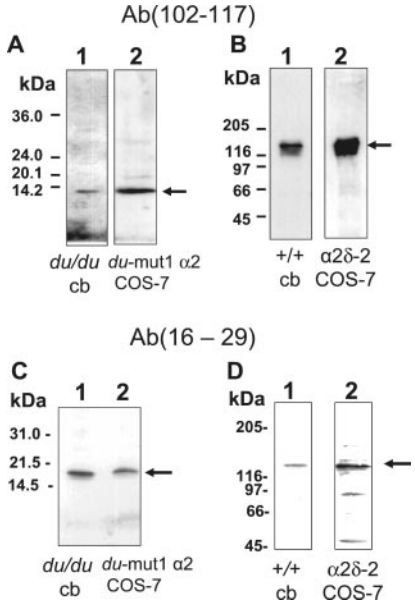

FIG. 6. **Immunopurification of *du*-mut1 α_2 from *du/du* cerebellum and the α_2 moiety of full-length α2δ-2 from +/+ cerebellum.** Immunoblot analysis of α2δ-2 proteins were immunocaptured from detergent-solubilized *du/du* or +/+ cerebellar membranes using column-immobilized peptide antibodies. Samples were separated on either 4–20% gradient gels (*A* and *B*), a 20% gel (*C*), or on a 7.5% gel (*D*). *Arrows* indicate the major protein bands detected. *A* and *C*, proteins from *du/du* cerebella (*lane 1*) or from COS-7 cells expressing *du*-mut1 α_2 (*lane 2*) isolated using Ab(102–117) and Ab(16–29), respectively. The respective apparent molecular mass values are ~10 and 16 kDa. *B* and *D*, proteins from +/+ cerebella (*lane 1*) or from COS-7 cells expressing full-length α2δ-2 (*lane 2*) isolated with Ab(102–117) and Ab(16–29), respectively. The respective apparent molecular mass values are 150 and 120 kDa.

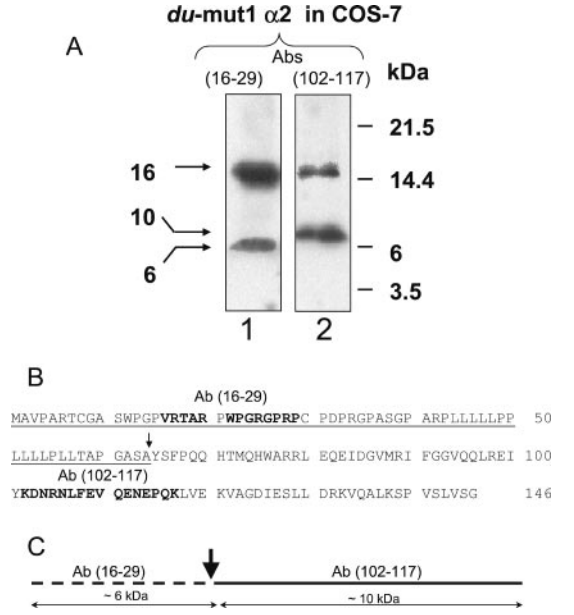

FIG. 7. **Processing of *du*-mut1 α_2.** *A*, immunoblot analysis of *du*-mut1 α_2 and fragments derived from cleavage of the signal peptide. Lysate (80 μg of protein) of COS-7 cells expressing *du*-mut1 α_2 was separated on a 10–20% gradient gel and probed with Ab(16–29) (*lane 1*) or Ab(102–117) (*lane 2*). A 16-kDa band is detected with both antibodies. Ab(16–29) also recognizes a band of 6 kDa, and Ab(102–117) recognizes a major band of ~10 kDa. *B*, amino acid sequence of *du*-mut1 α_2. The respective binding sites for Ab(16–29) and Ab(102–117) are shown in *bold*. The entire signal leader sequence is underlined with its predicted cleavage site marked by an *arrow* (40). *C* shows the calculated molecular mass values for *du*-mut1 α_2 (16 kDa) and the two proteolytic fragments as follows: *du*-mut1 α_2 following cleavage of the signal sequence (*solid line*, ~10 kDa) and the cleaved signal sequence (*dotted line*, ~6 kDa).

ther examined by PAGE of a larger amount (80 μg of protein) of COS-7 cell lysate expressing *du*-mut1 α_2, on a high percent gradient gel, followed by immunoblotting (Fig. 7*A*). A 16-kDa band was recognized by both antibodies, but the predominant band recognized by Ab(102–117) was ~10 kDa. This was not recognized by Ab(16–29), which recognized an additional 6-kDa band. The amino acid sequence of *du*-mut1 α_2 is shown in Fig. 7*B*, with the antibody recognition sites (*boldface letters*) and the predicted site of cleavage of the signal sequence (*arrow*). The predicted sizes of the peptides obtained before and after cleavage are 16 kDa for full-length *du*-mut1 α_2, 10 kDa for *du*-mut1 α_2 following cleavage of the signal sequence, and 6 kDa for the cleaved signal sequence (Fig. 7*C*), in agreement with the experimental results.

The immunolocalization of α2δ-2 in the cerebellum was subsequently examined using Ab(102–117). This antibody gave a pattern of immunostaining in the Purkinje cell layer (PCL) and molecular layer (ML) in sections of +/+ cerebellum, consistent with localization of α2δ-2 in PC bodies and dendrites (Fig. 8*A*, *left panel*). The staining was lost when the primary antibody was preincubated with the immunizing peptide or when the primary antibody was not used (Fig. 8*A*). In cerebellar sections from *du/du* mice, Ab(102–117) gave a low level of immunostaining (Fig. 8*A*, *right panel*), consistent with the presence of *du*-mut1 α_2 in *du/du* PCs. There was also some evidence for staining of Bergmann glia (Fig. 8*A*, *right panel* marked with *). We also used Ab(16–29) to determine where the uncleaved form of *du*-mut1 α_2 was expressed endogenously in *du/du* cerebellar sections. A low level of immunostaining was observed with this antibody in +/+ PCs, consistent with the presence of the immature 120-kDa form of α2δ-2, with the signal peptide still present, which is likely to be localized to the endoplasmic reticulum (Fig. 8*B*, *left panel*). Further evidence was obtained here for staining of Bergmann glia (Fig. 8*B*, *left panel*, *). In *du/du* cerebellum, we observed that immunostaining with this antibody was concentrated largely in the cell bodies of PCs (Fig. 8*B*, *right panel*). This is likely to represent the 16-kDa uncleaved *du*-mut1 α_2 species. The immunostaining was lost when the antibody was preincubated with the immunizing peptide (Fig. 8*B*). No differences were observed between +/+ and *du/du* PCs when Bergmann glia were visualized using an anti-glial fibrillary acidic protein antibody (results not shown).

Modulation of $Ca_V2.1$ Ca^{2+} Channel Currents by α2δ-2 and du-mut1 α_2—The possible pathological function of the *du*-mut1 α_2 protein encoded by the *Cacna2d2*^{du} gene was investigated using *in vitro* expression and electrophysiology. To mimic the PC complement of calcium channel subunits, the cDNAs corresponding to rat $Ca_V2.1$ and β_4 were transfected into COS-7 cells, with or without α2δ-2 or *du*-mut1 α_2 cDNA, and the resulting Ca_V currents (I_{Ba}) recorded. Co-expression of α2δ-2 increased $Ca_V2.1/\beta_4$ I_{Ba} currents, inducing a 2.9-fold enhancement of amplitude at 0 mV (Fig. 9*A*, and I-V relationships in Fig. 9*B*), with no significant shift in the voltage dependence of current activation (V_{50} for activation was -8.7 ± 0.7 mV ($n = 28$) for $Ca_V2.1/\beta_4$ and -10.7 ± 0.8 mV ($n = 42$) for $Ca_V2.1/\beta_4$/α2δ-2). There was no significant effect of α2δ-2 on the activation or inactivation of the $Ca_V2.1/\beta_4$ combination (Fig. 9*A* and results not shown).

In contrast, co-expression of *du*-mut1 α_2 induced a consistent reduction in $Ca_V2.1/\beta_4$ I_{Ba} amplitude throughout the voltage range (Fig. 9, *C* and *D*). This amounted to a 51% inhibition at 0 mV (Fig. 9*E*) and also resulted in a +5-mV shift in V_{50} for activation to -3.5 ± 1.1 mV ($n = 12$, $p < 0.01$ compared with $Ca_V2.1/\beta_4$). The mean current densities at 0 mV under the two

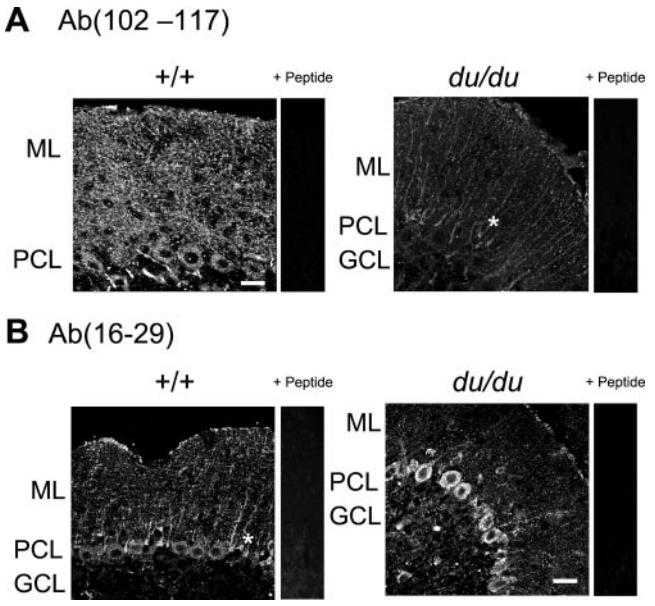

FIG. 8. **Immunohistochemistry in +/+ and *du*/*du* cerebellum.** *A*, Ab(102–117) detected the presence of α2δ-2 and *du*-mut1 α_2 protein in +/+ and *du*/*du* sections, respectively. The affinity of the antibody for α2δ-2 and *du*-mut1 α_2 may be different; therefore, relative intensities cannot be compared directly. Results are representative of four experiments. *B*, Ab(16–29) detected the presence of immature α2δ-2 in a +/+ cerebellar section (*left*) and *du*-mut1 α_2 protein in a *du*/*du* cerebellar section (*right*). Representative of three experiments. In both (*A* and *B*) the *calibration bar* is 30 μm. *ML*, molecular layer; *PCL*, Purkinje cell layer; *GCL*, granule cell layer. The label + peptide indicates that the primary antibody was preincubated with the immunizing peptide before application to the section. The * indicates examples of the presence of immunoreactivity in a smaller cell body and process, possibly a Bergmann glial cell.

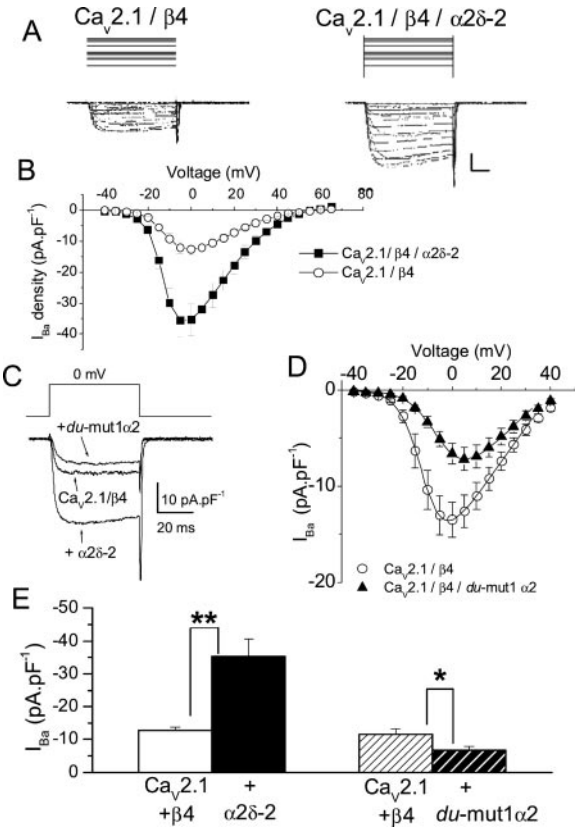

FIG. 9. **Enhancement of $Ca_V2.1/\beta_4$ currents by α2δ-2 and inhibition by *du*-mut1 α_2.** *A*, examples of I_{Ba} recorded from COS-7 cells transfected with $Ca_V2.1/\beta_4/\alpha2\delta$-2 or $Ca_V2.1/\beta_4$. The holding potential was −80 mV, and steps were to between −40 and +65 mV in 5-mV steps, delivered every 15 s. The charge carrier was 5 mM Ba^{2+}. The *scale bars* represent 10 pA·pF^{-1} and 10 ms. *B*, I–V relationships for $Ca_V2.1/\beta_4$ (○, $n = 28$) and $Ca_V2.1/\beta_4/\alpha2\delta$-2 (■, $n = 42$) peak I_{Ba} density in COS 7 cells. *C*, examples of the maximum I_{Ba} recorded at 0 mV from COS-7 cells transfected with $Ca_V2.1/\beta_4$, $Ca_V2.1/\beta_4/\alpha2\delta$-2, or $Ca_V2.1/\beta_4$/*du*-mut1 α_2, as in *A*. Co-expression of α2δ-2 induced a large enhancement of $Ca_V2.1/\beta_4$ I_{Ba}, whereas *du*-mut1 α_2 induced a reduction of $Ca_V2.1/\beta_4$ I_{Ba}. *D*, mean I–V relationships for $Ca_V2.1/\beta_4$ (○) and $Ca_V2.1/\beta$ 4/*du*-mut1 α_2 (▲) peak I_{Ba} density in COS-7 cells, fitted with a combined Boltzmann and linear function, as described under "Experimental Procedures." *E*, histogram of mean data, for the transfection conditions shown *below* the *bars*, from COS-7 cells. $Ca_V2.1/\beta_4$ (*open bar*, $n = 13$, controls for $Ca_V2.1/\beta_4/\alpha2\delta$-2 transfections); $Ca_V2.1/\beta_4/\alpha2\delta$-2 (*black bar*, $n = 42$); $Ca_V2.1/\beta_4$ (*open hatched bar*, $n = 15$, performed in parallel with $Ca_V2.1/\beta_4$/*du*-mut1 α_2 transfections) or $Ca_V2.1/\beta_4$/*du*-mut1 α_2 (*black hatched bar*, $n = 12$). Statistical significance of differences indicated given by *asterisks*: **, $p < 0.001$; *, $p < 0.05$ (Student's independent two tailed *t* test).

different conditions are compared in Fig. 9*E*. Similar results were obtained when these calcium channel subunits, in this case including rabbit Ca_V 2.1, were expressed in *Xenopus* oocytes (see Ref. 12 and data not shown).

Effect of α2δ-2 and du-mut1 α_2 on Single Ca^{2+} Channel Currents Formed by $Ca_V2.1$—We compared single channel parameters between cell-attached patches of COS-7 cells transfected with $Ca_V2.1/\beta_4$ cDNA, either without α2δ-2 (Fig. 10*A*) or co-expressed with either full-length α2δ-2 (Fig. 10*B*) or the *du*-mut1 α_2 (Fig. 10*C*). These experiments were performed in order to differentiate between a mechanism that involves changing the biophysical properties of Ca_V 2.1 channels and a mechanism that involves changing the trafficking or membrane expression levels of the Ca_V 2.1 channels, imposed by either α2δ-2 or *du*-mut1 α_2.

Once opened, Ca_V 2.1 channels showed an average single channel conductance of 9.9 ± 0.4 pS ($n = 8$) for $Ca_V2.1/\beta_4$, which was not significantly affected by co-expression of α2δ-2 (10.2 ± 0.6 pS, $n = 8$) or *du*-mut1 α_2 (8.8 ± 1.0 pS, $n = 6$) (Fig. 10*D*, *left*). This conductance is similar to that of P-type channels recorded from wild-type and *du*/*du* PCs under the same conditions (12). More detailed analysis demonstrated openings to three distinct amplitude levels, as has also been shown in native Purkinje cells (28), level 2 being the most prominent in our recordings (Fig. 10*D*, *middle* and *right*, see legend for conductance and amplitude values). Neither the conductance nor the amplitude of the three current levels was significantly affected by expression of α2δ-2 or *du*-mut1 α_2 (data not shown).

Neither α2δ-2 nor *du*-mut1 α_2 caused any significant change in mean open or closed times or in the pattern of voltage dependence of Ca_V 2.1 channels (Fig. 10*E*). We also examined the activation kinetics by measuring the latency to first opening of the channels in response to a square voltage pulse (Fig. 10*F*). Ca_V 2.1 channel activation was not influenced by the subunits examined (Fig. 10*F*, *left*), at any voltage (Fig. 10*F*, *right*). In addition, the voltage dependence of inactivation (Fig. 10*G*) was not influenced by either α2δ-2 or *du*-mut1 α_2.

Although the presence of α2δ-2 caused an ~3-fold increase in whole cell current amplitude, all the single channel parameters were indistinguishable between the three conditions. This implies that the basic active unit in the whole cell current (an individual channel) remains unchanged, and the modulation by α2δ-2 must involve an alteration in the number of active channels in the membrane.

DISCUSSION

PCs from du/du Mice Have a Reduced Dendritic Arbor—PC somata form a monolayer by 10 days postnatally in the mouse, and their dendrites reach the pial surface at day 20, coinciding with the completion of granule cell migration and concomitant parallel fiber production (29). The PC soma typically exhibits one primary dendrite, which emerges apically, and one axonal

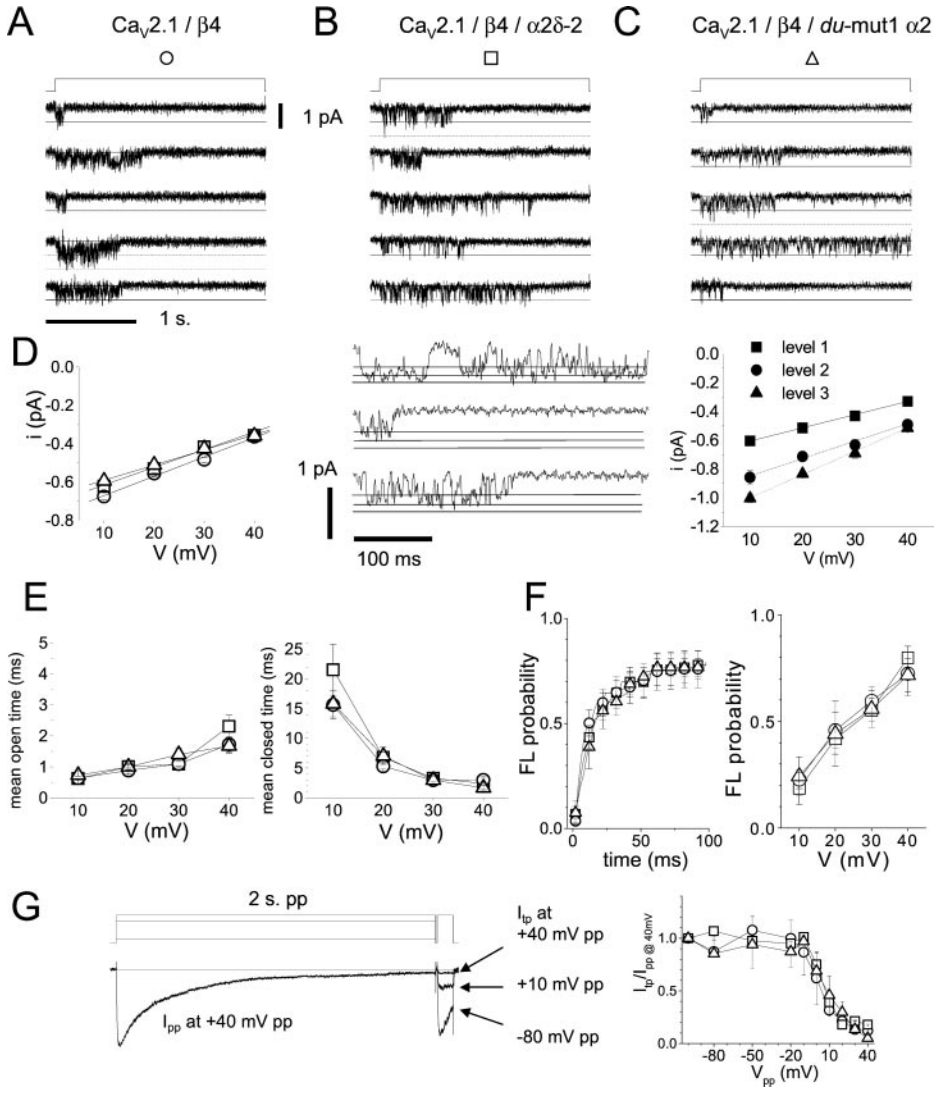

FIG. 10. **Comparison between the effect of α2δ-2 or *du*-mut1 α_2 on single channel parameters of Ca$_V$2.1.** *A*, single channel activity (maximum of two simultaneous overlapping openings) of Ca$_V$2.1/β_4 without the α2δ-2 auxiliary subunit. *Top*, the voltage protocol: holding potential −100 mV. A 2-s-long pulse, here to +30 mV, delivered every 10 s. *Bottom*, 5 representative traces of single channel activity. *Openings* are downward deflections, and a *continuous line* marks both the closed and open states, in traces with overlapping openings an additional *dashed line* marks the second level. *B*, single channel activity (maximum of two simultaneous overlapping openings) arising from Ca$_V$2.1/β_4 co-expressed with the α2δ-2 auxiliary subunit. Format as in *A*. *C*, single channel activity (maximum of two simultaneous overlapping openings) arising from Ca$_V$2.1/β_4 co-expressed with the *du*-mut1 α_2. Format as in *A*. *D*, *left*, average single channel conductance for the 3 conditions depicted in *A–C* (○, $n = 8$; □, $n = 8$; △, $n = 6$), respectively. Conductance was determined by linear fits to the data shown. See text for mean fit values. *Middle*, examples of single channel activity at +30 mV for Ca$_V$2.1/β_4 where more than one amplitude level was observed. *Continuous lines* mark the three amplitude levels, depicted by: ■, level 1; ●, level 2; ▲, level 3 on *right*. *Right*, single channel I–V plot to show the distinct conductances for data such as that shown. The single channel conductances for the three levels are 8.2 ± 1.2, 12.1 ± 1.05, and 16.2 ± 0.46 pS ($n = 6$), and the corresponding amplitudes at +30 mV are −0.43 ± 0.027, −0.63 ± 0.038, and −0.69 ± 0.033 pA. *E*, mean open (*left*) and closed (*right*) times were similar at all voltages examined, for the three conditions, respectively (○, $n = 8$; □, $n = 8$; △, $n = 6$). *F*, FL probability histogram, for the three conditions, respectively (○, $n = 8$; □, $n = 8$; △, $n = 5$). *Left*, mean (± S.E., shown every 10 ms for clarity) cumulative FL probability distributions at +30 mV, and *right*, FL probability at 20 ms for all voltages examined. *G*, steady-state inactivation of Ca$_V$ 2.1 ensemble currents from single and multichannel patches. *Left*, an example of inactivation experiment. *Top*, the voltage protocol, holding potential, −100 mV, followed by a 2 s. Prepulse (*pp*) to a potential (V_{pp}) between −80 and +40 mV, followed by a test pulse to +40 mV for 100 ms. *Bottom*, average ensemble currents (from the data as shown in *B* with a V_{pp} of +40 mV (*left*) and test pulse responses to V_{pp} of −80, +10, and +40 mV are superimposed. *Right*, all currents were normalized to the peak prepulse current at +40 mV and the ratio plotted as a function of V_{pp}. Data of the type shown in (*A–C*), respectively (○, $n = 11$; □, $n = 11$; △, $n = 4$).

process projecting in the opposite direction. The PC dendritic trees develop most dramatically between postnatal day 9 and 20, reaching 80% of their adult dimension in this period (30). PCs from *du*/*du* mice appear immature, reduced both in size and complexity, with multiple primary dendrites and small arbors that often terminate well below the pial surface. Thickened secondary and tertiary dendritic trunks are also present. The multipolar appearance of some of the *du*/*du* PCs may be a remnant of their immature stage (in which the normal resorption of all somatic filopodia fails to occur), with some of these processes continuing to develop into dendrites as found in weaver and staggerer mouse mutants (31).

Thus, although we have shown that PCs are not lost in *du*/*du* cerebella at P21 (12), we now find that the PC dendritic tree is reduced in size and shows other abnormalities, such as weeping willow dendrites and dendritic thickening. Similar abnormalities have been found in a number of the spontaneously occurring Ca$_V$ 2.1 mouse mutants (8), and some of these (in particular tg^{la}) also show PC loss in older mice (32). The mechanism of the altered PC morphology in *du*/*du* mice may result

either from the reduced PC calcium channel currents, which we observed in P5-P9 PCs, before the extensive growth of the dendritic arbor (12) or more directly from the loss of α2δ-2, with the possible additional consequences of expression of a truncated mutant α_2 protein. A number of the human genetic diseases involving $Ca_V2.1$, for example familial hemiplegic migraine (33), cerebellar ataxia, and PC degeneration are associated with mutations that have been shown to produce a reduction in $Ca_V2.1$ calcium currents *in vitro* (34). However, the mechanism whereby such molecular changes are translated into morphological and functional abnormalities remains to be determined.

A Truncated Mutant Protein Derived from the 5′ Mutant Transcript of Cacna2d2 Is Expressed in du Mice—The *in situ* hybridization study demonstrates that although wild-type *Cacna2d2* transcript is absent from the brain of *du*/*du* mice, because of the genomic rearrangement that disrupts *Cacna2d2* (12), a 5′ mutant transcript (*du* mutant transcript 1) is present in *du*/*du* PCs. This transcript is predicted to encode a protein (*du*-mut1 α_2) that lacks most of the α_2 subunit and the whole of the δ subunit, including its transmembrane domain. It is frequently the case that mRNA encoding mutant transcripts, where a frameshift or point mutation introduces one or more premature stop or nonsense codons, is unstable and subject to nonsense-mediated mRNA decay (35). Indeed, although a second mutant transcript 2, predicted to be formed from exons 2–39, was identified by reverse transcriptase-PCR and Northern blot in *du*/*du* mouse brain, it was not observed by *in situ* hybridization in *du*/*du* PCs (12). Furthermore, the 5′ *du* mutant transcript 1 appeared to be present at a low level in *du*/*du* brain (12). To determine whether this mutant transcript was translated, we used two α2δ-2 anti-peptide antibodies, which were raised against peptides within the *du*-mut1 α_2 sequence, Ab(16–29) and Ab(102–117).

It has been established, from studies with site-directed antipeptide antibodies, that the topology of the α2δ-1 subunit is such that the α_2 subunit, which has an N-terminal leader signal sequence, is entirely extracellular (36–38). The α_2 subunit is disulfide-bonded to a transmembrane δ subunit, and both subunits have been found to be involved in the interaction with the $Ca_v1.2$ subunit (38, 39). Now that two other α2δ subunit genes have been cloned, it is assumed that they have the same topology, and indeed, high homology is present between the N termini of α2δ-1 and α2δ-3, with the clear prediction of a cleaved signal peptide in both sequences. In contrast, although a putative signal peptide is found in α2δ-2, it is much longer. By using prediction analysis, it is found to have a potential cleavage site after position 64 (40) (Fig. 7*B*), whereas only 2% of eukaryotic signal peptides are longer than 35 residues (40). In particular, it has a longer sequence N-terminal to the putative hydrophobic signal sequence (~42 amino acids) than α2δ-1 or α2δ-3 (which are ~3 and 11 amino acids, respectively). Such "*n* regions" are found to be less than 25 amino acids in 80% of secreted or transmembrane proteins where they occur (41). Therefore, it remains unclear whether this signal sequence is cleaved efficiently, as cleavage is often delayed when the signal sequence is long (42). This results in extended transit times through the endoplasmic reticulum-Golgi apparatus, which may be required for highly glycosylated proteins (42). Such an explanation is likely to be the reason for our observation using Ab(16–29), of a 120-kDa immunolabeled protein when α2δ-2 was expressed in COS-7 cells. This is likely to represent the α_2 moiety of full-length α2δ-2 (predicted protein molecular mass of 113 kDa), which is immature in that it has an uncleaved signal peptide and, judging by the molecular weight, no added carbohydrate.

It appears that in the case of *du*-mut1 α_2 expressed in COS-7 cells, the truncated protein is processed such that the signal sequence remains at least in part uncleaved, because both Ab(16–29) and Ab(102–117) recognized a band of ~16 kDa, the predicted size for the uncleaved *du*-mut1 α_2, and Ab(16–29) also recognized a fainter band of about 6 kDa, which would represent the cleaved signal peptide. However, the predominant band recognized by Ab(102–117) but not Ab(16–29) was a ~10-kDa protein, which is therefore likely to represent *du*-mut1 α_2 with its signal peptide cleaved. This result corresponded exactly with the molecular weight of the native *du*-mut1 α_2 immunocaptured from *du*/*du* cerebellum by the same antibody, indicating that it is a stable *in vivo* species in these mice. This study also confirmed the previous indication (12) that *du* mutant transcript 2, which would be recognized by Ab(102–117), is not translated. A 16-kDa protein was immunocaptured by Ab(16–29) from *du*/*du* cerebellum, indicating that the signal sequence remains, in part, uncleaved from *du*-mut1 α_2. The reason that this species was not also immunocaptured by Ab(102–117) may indicate that Ab(102–117) is of lower affinity, as also suggested by the data in Fig. 8.

Immunolocalization of α2δ-2 and du-mut1 α_2 in Cerebellum—In cerebellar sections, we found, using Ab(102–117), that α2δ-2 is expressed in wild-type PC somata and also in the ML of the cerebellum, suggesting localization in PCs. It is also possible that some of the immunostaining arises from cerebellar afferents or from Bergmann glia, and this will be investigated in the future. In *du*/*du* cerebellum, a low level of immunostaining was observed with the same antibody. These results support the finding that *du*-mut1 α_2 is expressed in *du*/*du* cerebellum. Immunoreactivity in *du*/*du* cerebellar sections was also observed using Ab(16–29), where staining, presumably representing the uncleaved *du*-mut1 α_2, was concentrated in PC somata. In agreement with the expression study in COS-7 cells and the immunopurification data from cerebellum, this suggests that *du*-mut1 α_2 retains, in part, the putative signal sequence at its N terminus and does not appear to be secreted. When *du*-mut1 α_2 was expressed in COS-7 cells both Ab(16–29) and Ab(102–117) recognized an epitope that was only expressed intracellularly, indicating that *du*-mut1 α_2 is unlikely to be secreted or inserted into the plasma membrane as a transmembrane protein.

The Functional Interaction of the $Ca_V2.1/\beta_4$ Combination with α2δ-2—The similarity of the ducky phenotype to that observed in mice with mutations in genes encoding the $Ca_V2.1$ (7) and β_4 (9) subunits and their predominant PC expression pattern suggests that α2δ-2 contributes to the P-type current. This is reinforced by our finding that the currents formed by both rat and rabbit $Ca_V2.1$ co-expressed with β_4, which is the main PC β subunit, were strongly enhanced by α2δ-2, in two expression systems (COS-7 cells and *Xenopus* oocytes).

Previous *in vitro* studies have shown that α2δ-1, α2δ-2, and α2δ-3 subunits act to increase the maximum conductance of a number of expressed calcium channel α_1/β subunit combinations at the whole cell level (2, 43–46). However, this may be dependent to some extent on the specific combination of α_1 and β subunits expressed. Furthermore, the effects of α2δ subunits on kinetics and voltage dependence of activation are more minor (2, 44). We have also investigated this for the calcium channel subunit combinations used in the present study, and we show that α2δ-2 had no influence on voltage-dependent properties and had no effect on single channel conductance or other biophysical parameters of the $Ca_V2.1/\beta_4$ channels themselves. This implies that α2δ-2 probably has its main effect on the lifetime of the channel complex in the plasma membrane, either by enhancing trafficking or reducing turnover. In agree-

ment with this proposed mechanism, it has previously been found that $\alpha 2\delta$-1 increased the amount of $Ca_V1.2$ protein expressed in *Xenopus* oocytes (47).

In contrast, the protein product of *du* mutant transcript 1, *du*-mut1 α_2, produced a consistent reduction in $Ca_V2.1/\beta_4$ currents in COS-7 cells. Thus, whereas loss of full-length α 2δ-2 is likely to be the most important contributing factor, the expression of the truncated *du*-mut1 α_2 may also contribute to the *du*/*du* phenotype, via an additional suppressive effect, possibly by interfering with the correct trafficking of α_1 subunits.

Acknowledgments—We thank Professor R. M. Gardiner for support and encouragement. We also thank Dr. Kevin Bittman, Dr. David Becker, and Dr. Marina Mione for generously sharing their expertise and Mick Keegan for excellent technical assistance.

REFERENCES

1. Catterall, W. A. (2000) *Annu. Rev. Cell Dev. Biol.* **16,** 521–555
2. Walker, D., and De Waard, M. (1998) *Trends Neurosci.* **21,** 148–154
3. Letts, V. A., Felix, R., Biddlecome, G. H., Arikkath, J., Mahaffey, C. L., Valenzuela, A., Bartlett, F. S., Mori, Y., Campbell, K. P., and Frankel, W. N. (1998) *Nat. Genet.* **19,** 340–347
4. Chen, L., Chetkovich, D. M., Petralia, R. S., Sweeney, N. T., Kawasaki, Y., Wenthold, R. J., Bredt, D. S., and Nicoll, R. A. (2000) *Nature* **408,** 936–943
5. Ertel, E. A., Campbell, K. P., Harpold, M. M., Hofmann, F., Mori, Y., Perez-Reyes, E., Schwartz, A., Snutch, T. P., Tanabe, T., Birnbaumer, L., Tsien, R. W., and Catterall, W. A. (2000) *Neuron* **25,** 533–535
6. Burgess, D. L., Gefrides, L. A., Foreman, P. J., and Noebels, J. L. (2001) *Genomics* **71,** 339–350
7. Fletcher, C. F., Lutz, C. M., O'Sullivan, T. N., Shaughnessy, J. D., Jr., Hawkes, R., Frankel, W. N., Copeland, N. G., and Jenkins, N. A. (1996) *Cell* **87,** 607–617
8. Zwingman, T. A., Neumann, P. E., Noebels, J. L., and Herrup, K. (2001) *J. Neurosci.* **21,** 1169–1178
9. Burgess, D. L., Jones, J. M., Meisler, M. H., and Noebels, J. L. (1997) *Cell* **88,** 385–392
10. Kang, M. G., Chen, C. C., Felix, R., Letts, V. A., Frankel, W. N., Mori, Y., and Campbell, K. P. (2001) *J. Biol. Chem.* **276,** 32917–32924
11. Sharp, A. H., Black, J. L., III, Dubel, S. J., Sundarraj, S., Shen, J. P., Yunker, A. M. R., Copeland, T. D., and McEnery, M. W. (2001) *Neuroscience* **105,** 599–617
12. Barclay, J., Balaguero, N., Mione, M., Ackerman, S. L., Letts, V. A., Brodbeck, J., Canti, C., Meir, A., Page, K. M., Kusumi, K., PerezReyes, E., Lander, E. S., Frankel, W. N., Gardiner, R. M., Dolphin, A. C., and Rees, M. (2001) *J. Neurosci.* **21,** 6095–6104
13. Snell, G. D. (1955) *J. Hered.* **46,** 27–29
14. Meier, H. (1968) *Acta Neuropathol.* (*Berl.*) **11,** 15–28
15. Stuart, G. J., Dodt, H. U., and Sakmann, B. (1993) *Pfluegers Arch. Eur. J. Physiol.* **423,** 511–518
16. Eisenstat, D. D., Liu, J. K., Mione, M., Zhong, W. M., Yu, G. Y., Anderson, S. A., Ghattas, I., Puelles, L., and Rubenstein, J. L. R. (1999) *J. Comp. Neurol.* **414,** 217–237
17. Brice, N. L., Berrow, N. S., Campbell, V., Page, K. M., Brickley, K., Tedder, I., and Dolphin, A. C. (1997) *Eur. J. Neurosci.* **9,** 749–759
18. Macart, M., and Gerbaut, L. (1982) *Clin. Chim. Acta* **122,** 93–101
19. Berrow, N. S., Brice, N. L., Tedder, I., Page, K., and Dolphin, A. C. (1997) *Eur. J. Neurosci.* **9,** 739–748
20. Hans, M., Urrutia, A., Deal, C., Brust, P. F., Stauderman, K., Ellis, S. B., Harpold, M. M., Johnson, E. C., and Williams, M. E. (1999) *Biophys. J.* **76,** 1384–1400
21. Barclay, J., and Rees, M. (2000) *Mamm. Genome* **11,** 1142–1144
22. Cormack, B. P., Valdivia, R. H., and Falkow, S. (1996) *Gene* (*Amst.*) **173,** 33–38
23. Meir, A., Bell, D. C., Stephens, G. J., Page, K. M., and Dolphin, A. C. (2000) *Biophys. J.* **79,** 731–746
24. Canti, C., Page, K. M., Stephens, G. J., and Dolphin, A. C. (1999) *J. Neurosci.* **19,** 6855–6864
25. Meir, A., and Dolphin, A. C. (1998) *Neuron* **20,** 341–351
26. Neher, E. (1995) in *Single-channel Recording* (Sakmann, B., and Neher, E., eds) pp. 147–153, Plenum Publishing Corp., New York
27. Imredy, J. P., and Yue, D. T. (1994) *Neuron* **12,** 1301–1318
28. Usowicz, M. M., Sugimori, M., Cherksey, B., and Llinαs, R. (1992) *Neuron* **9,** 1185–1199
29. Fujita, S. (1967) *J. Cell Biol.* **32,** 272–288
30. Sadler, M., and Berry, M. (1984) *Proc. R. Soc. Lond. Ser. B Biol. Sci.* **221,** 349–367
31. Sotelo, C. (1975) *Adv. Neurol.* **12,** 335–351
32. Heckroth, J. A., and Abbott, L. C. (1994) *Brain Res.* **658,** 93–104
33. Ophoff, R. A., Terwindt, G. M., Vergouwe, M. N., van Eijk, R., Oefner, P. J., Hoffman, S. M., Lamerdin, J. E., Mohrenweiser, H. W., Bulman, D. E., Ferrari, M., Haan, J., Lindhout, D., van Ommen, G. J., Hofker, M. H., Ferrari, M. D., and Frants, R. R. (1996) *Cell* **87,** 543–552
34. Hans, M., Luvisetto, S., Williams, M. E., Spagnolo, M., Urrutia, A., Tottene, A., Brust, P. F., Johnson, E. C., Harpold, M. M., Stauderman, K. A., and Pietrobon, D. (1999) *J. Neurosci.* **19,** 1610–1619
35. Culbertson, M. R. (1999) *Trends Genet.* **15,** 74–80
36. Brickley, K., Campbell, V., Berrow, N., Leach, R., Norman, R. I., Wray, D., Dolphin, A. C., and Baldwin, S. (1995) *FEBS Lett.* **364,** 129–133
37. Gurnett, C. A., De Waard, M., and Campbell, K. P. (1996) *Neuron* **16,** 431–440
38. Gurnett, C. A., Felix, R., and Campbell, K. P. (1997) *J. Biol. Chem.* **272,** 18508–18512
39. Felix, R., Gurnett, C. A., De Waard, M., and Campbell, K. P. (1997) *J. Neurosci.* **17,** 6884–6891
40. Nielsen, H., Engelbrecht, J., Brunak, S., and vonHeijne, G. (1997) *Protein Eng.* **10,** 1–6
41. Martoglio, B., and Dobberstein, B. (1998) *Trends Cell Biol.* **8,** 410–415
42. Li, Y., Luo, L. Z., Thomas, D. Y., and Kang, C. Y. (1994) *Virology* **204,** 266–278
43. Mori, Y., Friedrich, T., Kim, M.-S., Mikami, A., Nakai, J., Ruth, P., Bosse, E., Hofmann, F., Flockerzi, V., Furuichi, T., Mikoshiba, K., Imoto, K., Tanabe, T., and Numa, S. (1991) *Nature* **350,** 398–402
44. Klugbauer, N., Lacinova, L., Marais, E., Hobom, M., and Hofmann, F. (1999) *J. Neurosci.* **19,** 684–691
45. Dolphin, A. C., Wyatt, C. N., Richards, J., Beattie, R. E., Craig, P., Lee, J.-H., Cribbs, L. L., Volsen, S. G., and Perez-Reyes, E. (1999) *J. Physiol.* (*Lond.*) **519,** 35–45
46. Hobom, M., Dai, S., Marais, E., Lacinova, L., Hofmann, F., and Klugbauer, N. (2000) *Eur. J. Neurosci.* **12,** 1217–1226
47. Shistik, E., Ivanina, T., Puri, T., Hosey, M., and Dascal, N. (1995) *J. Physiol.* (*Lond.*) **489,** 55–62